



Physical-aware Radar Image Synthesis with Projective Network

Qian Song⁽¹⁾, and Feng Xu^{*(2)} and Xiao Xiang Zhu⁽¹⁾

(1) Remote Sensing Technology Institute, German Aerospace Center, Wessling, Germany, 82234

(2) Key Laboratory for Information Science of Electromagnetic Waves (MoE), Fudan University, Shanghai, China, 200433

Abstract

This paper proposed a new network module named as projection network. It assumes that each 2D radar cross section (RCS) map is a projection of a 3D RCS map. And it models the projection mechanism as a differentiable layer, so that it can be integrated with other neural network layers, such as convolutional and pooling layers. The proposed model is consistent with radar projection process, hence effects such as layover is considered. It is designed and used specifically for radar applications. This paper applied the proposed network on radar image synthesis, and the simulation results showed great potential of projective network.

1 Introduction

Radar image synthesis has been widely applied on Zero-/Few-shot learning, semi-supervised learning of radar targets [1-4]. Usually the generative networks are feed with the attributes (such as labels and orientations) of the targets, and output the radar images. Thus training the generators using limited number of data itself is challenging due to the complex imaging mechanisms of radar.

In [5], as inspired by human's one-shot learning ability, Lake et al. combined the ideas of compositionality, causality, and learning to learn, and proposed Bayesian program learning framework that is able to learn rich concepts from single example. It implies that introducing physical-aware model into deep learning framework has the potential to boost the radar applications. In [6], Zhang et al. proposed a complex-valued convolutional neural networks (CV-CNN) in order to take advantage of the phase information of synthetic aperture radar data. In order to address the InSAR image synthesis problem, Nyquist mapping is proposed to convert the input complex-valued data into real data to fit the cGAN [4]. In [5], Wei and Chen proposed an cascaded convolutional neural network with skip connection that takes the advantage of the traditional iterative algorithms. But in these papers, the used modules and architectures are taken from traditional convolutional neural networks.

In this paper, we makes an attempt to mimic the radar's projection process and proposes a new network module named projection layer. It can be applied to multiple radar applications when coupled with deep learning techniques. Here

we took image synthesis as an example. We assume that a 3D radar cross section (RCS) model exists that any 2D RCS map is a projection of it at given observation angle. Using the training 2D RCS image, the 3D RCS can be estimated, and then 2D RCS map at other observation angle can be generated through projection. Via taking point spread function (PSF), the projection network is differentiable, thus the 3D RCS can be inversed using standard optimizers.

2 Projection Model

This section introduces the projection module, and its forward propagation process as well as results. In order to make the module differentiable, point spread function is used when rasterization.

2.1 Assumption

The projection network learns a 3D RCS representation based on single 2D RCS map. The corresponding relationship between RCS σ_{ij} and the scattering coefficient S_{ij} is

$$\sigma_{ij} = 4\pi |S_{ij}|^2 \quad (1)$$

where, $i, j \in \{h, v\}$ refer to the polarization of scattering and incident electromagnetic wave. Only the single polarimetry case is considered in this paper. The proposed projection network is based on the following assumption: a 3D RCS of the target exists. It corresponds to a 3D matrix, where the value of each element is a synthetic representation of the corresponding target point; any 2D RCS map is a projection of it at the specific observation angle. There is no such 3D RCS in practice. This concept is further simplified as a combination of the 2D synthetic RCS namely $\boldsymbol{\sigma}_s \in \mathbb{R}^{m,n}$ and height distribution matrix $\mathbf{H} \in \mathbb{R}^{m,n}$.

2.2 Forward Propagation

Suppose the synthetic RCS and height of the target are $\boldsymbol{\sigma}_s$ and \mathbf{H} ; let the ground range and azimuth between each point and the reference point be X, Y ; the depression angle of emitted electromagnetic wave is θ ; and the orientation angle of the target is ϕ . Forward propagation of projective network is to get the projected 2D RCS $\boldsymbol{\sigma} = \{\sigma_{ij}\}$. It can be divided into two steps: rotate the height matrix according to the the depression angle and the orientation first, and

then rasterization, as illustrated in Figure 1. Height, slant range and vertical slant range after rotation are represented by H' , X' , Y' . Then we have

$$\begin{bmatrix} X' \\ Y' \\ H' \end{bmatrix} = \begin{bmatrix} \cos \theta \cos \phi & -\cos \theta \sin \phi & -\sin \theta \\ \sin \phi & \cos \phi & 0 \\ \sin \theta \cos \phi & -\sin \theta \sin \phi & \cos \theta \end{bmatrix} \begin{bmatrix} X \\ Y \\ H \end{bmatrix} \quad (2)$$

Then the 2D of each resolution cell is allocated according to the rotated data, i.e. rasterization. Here the shadow effect that the tall near-range target blocks the short far-range target isn't took into consideration, thus H' is ignored. Then the RCS at slant range x and vertical range y is

$$\sigma_{ij} = \vec{\sigma}_s^T f(x - \vec{X}', y - \vec{Y}') \quad (3)$$

where, \vec{X}' means vectorization of X' . To make rasterization differentiable, the point spread function is introduced here as a two-dimensional Gaussian function,

$$f(x, y) = \exp^{-\lambda(x^2 + y^2)} \quad (4)$$

Here λ in PSF is set as 4.

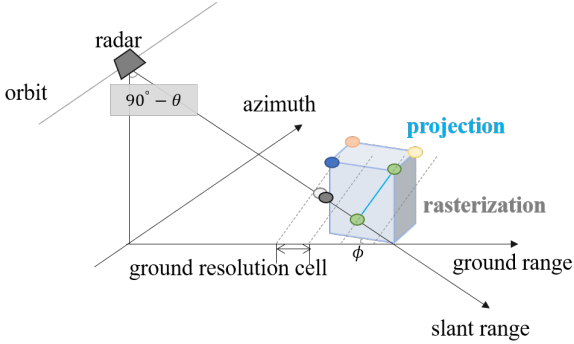


Figure 1. Illustration of projection and rasterization processes.

2.3 Simulation Results

Simulated data are used as an example. The forward propagation of the network is to output the 2D RCS map given a synthetic three-dimensional RCS. The simulated 3D RCS model considered in this paper is shown in Figure 2. The targets consist of three cuboids, which represents two adjacent buildings with different architectures, heights and shapes. The height of the background, and the three cuboids are set as 1, 4 (red one), 2 (yellow one), and 1.5 (green one) times of the resolution respectively.

As mentioned before, it is actually represented by a synthetic RCS, and height distribution map. Figure 3 and Figure 4 compared the projected results with and without (which is considered as the ground-truth) using point spread function. Although significant difference remains, both images show similar target profiles and distributions of strong scattering points.

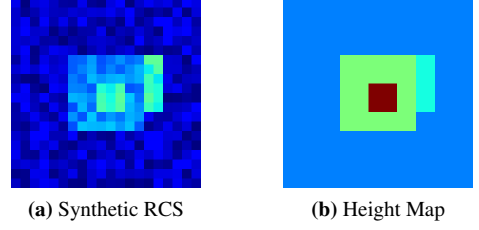


Figure 2. The simulated synthetic RCS (a) and the height (b) of the target.

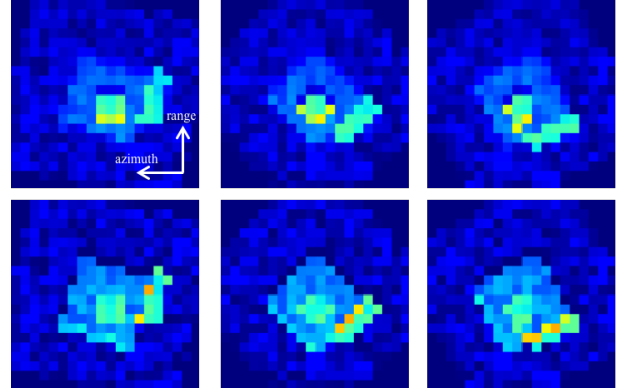


Figure 3. Projected 2D RCS images via projective network with (top row) and without (bottom row) using point spread function: (left) $\theta = 15^\circ$, $\phi = 15^\circ$; (middle) $\theta = 15^\circ$, $\phi = 45^\circ$; (right) $\theta = 15^\circ$, $\phi = 60^\circ$.

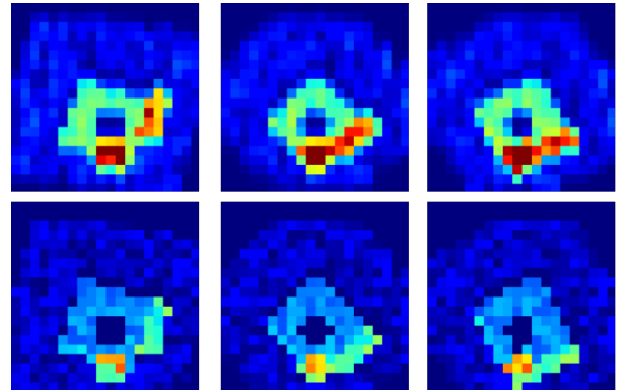


Figure 4. Projected 2D RCS images via projective network with (top row) and without (bottom row) using point spread function: (left) $\theta = 60^\circ$, $\phi = 15^\circ$; (middle) $\theta = 60^\circ$, $\phi = 45^\circ$; (right) $\theta = 60^\circ$, $\phi = 60^\circ$.

3 Image Synthesis with Projection Network

3.1 Parameters Estimation

Now that the proposed projective network is differentiable, the 3D RCS, i.e. σ_s and \mathbf{H} , can be retrieved through standard optimizers that based on back-propagation algorithms. Based on our experience, retrieval of the two matrix simultaneously is challenging, thus we assume that the \mathbf{H} is known. Denote the projective network as \mathcal{F} , then the loss function is defined as,

$$L = \|\mathcal{F}(\sigma_s|\mathbf{H}) - \sigma\|_2^2 \quad (5)$$

σ_s is firstly randomly initialized; and then through back-propagation the gradients of the loss with regard to the outputs (in Equation (6)) for certain iterations, σ_s will be ungraded and optimized via Equation (7)~(10).

$$\nabla\sigma_s = \frac{\partial L}{\partial \mathcal{F}(\sigma_s|\mathbf{H})} \frac{\partial \mathcal{F}(\sigma_s|\mathbf{H})}{\partial \sigma_s} \quad (6)$$

$$\mathbf{m}_t = \beta_1 \mathbf{m}_{t-1} + (1 - \beta_1) \nabla\sigma_s \quad (7)$$

$$\mathbf{v}_t = \beta_2 \mathbf{v}_{t-1} + (1 - \beta_2) \nabla\sigma_s^2 \quad (8)$$

$$\hat{\mathbf{m}}_t = \frac{\mathbf{m}_t}{1 - \beta_1^t}, \quad \hat{\mathbf{v}}_t = \frac{\mathbf{v}_t}{1 - \beta_2^t} \quad (9)$$

$$\sigma_s^{i+1} = \sigma_s^i - \frac{\eta \hat{\mathbf{m}}_t}{\sqrt{\hat{\mathbf{v}}_t} + \varepsilon} \quad (10)$$

Where $\beta_1 = 0.9$, $\beta_2 = 0.999$, $\varepsilon = 10^{-8}$ and $\eta = 0.001$. It is worth noting that the projection network is a non-parameter model, which makes it sensitive to the quality of training data. In this paper, the projective network is trained with single sample (shown in Figure 5(c)) to show its FSL ability.

Figure 5 shows the retrieved synthetic RCS, and compared the reconstructed 2D RCS with the training image. Based on the results, the reconstruction error is ignorable. The R^2 and mean relative error (MRE) of the recovered synthetic RCS is 0.69 and 1.67 respectively. Based on the results in the next subsection, this amount of error is acceptable for image synthesis. From the results, the retrieval error of target area is larger than that of background area, due to the layover effect.

Due to the layover effect, the estimation error is related with the training sample chosen. Smaller orientation and depression angle brings less deformation and layover effect, thus will result in smaller estimation error. As an example, Figure 6 and Table 1 compared the recovered synthetic RCS, R^2 and MRE using training samples of different orientation angles. From the results, we can see that the estimation error grows with increase of orientation angle.

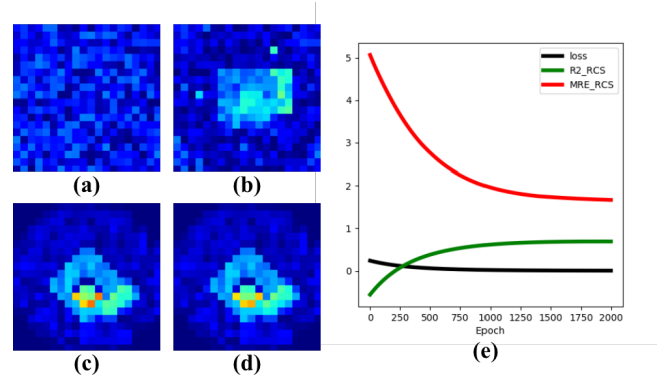


Figure 5. (a) The randomly initialized synthetic RCS; (b) retrieved synthetic RCS using single training sample of $\theta = 30^\circ$, $\phi = 45^\circ$ (c); (d) the reconstructed projected image; (e) the loss, and R-square of the retrieved and real synthetic RCS, as well as the mean relative error along training.

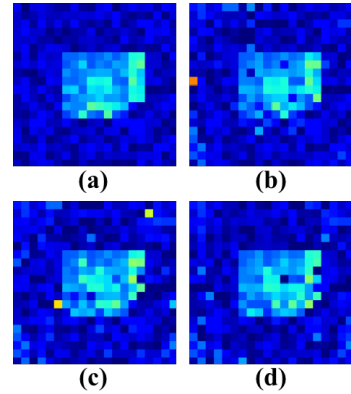


Figure 6. Recovered synthetic RCS using the training sample with (a) $\phi = 0^\circ$; (b) $\phi = 15^\circ$; (c) $\phi = 30^\circ$; (d) $\phi = 60^\circ$.

Table 1. Comparison of estimation results using training sample of different orientation angles.

ϕ	0°	15°	30°	45°	60°
R^2	0.93	0.61	0.46	0.69	0.57
MRE	0.11	1.22	1.61	1.67	1.84

3.2 Image Synthesis

The retrieved synthetic RCS in Figure 5 is used in this subsection to synthesize 2D RCS images at other observation angles. The results are shown in Figure 7 and Figure 8. The reconstructed images show similar target profile as real ones, but the strong scattering points are wrongly placed. The reconstruction error of the first two columns are larger than that of other examples. It reveals that the main challenge underlying the image synthesis is the shifted features of targets under different orientation angles.

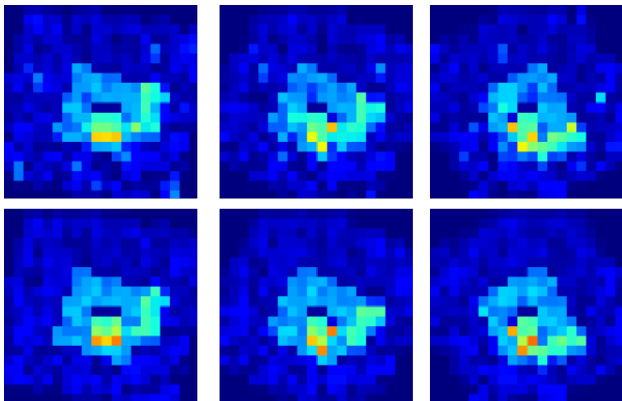


Figure 7. Generated images via trained projective network (top row) and the corresponding simulated radar images (bottom row): (left) $\theta = 30^\circ$, $\phi = 15^\circ$; (middle) $\theta = 30^\circ$, $\phi = 30^\circ$; (right) $\theta = 30^\circ$, $\phi = 60^\circ$.

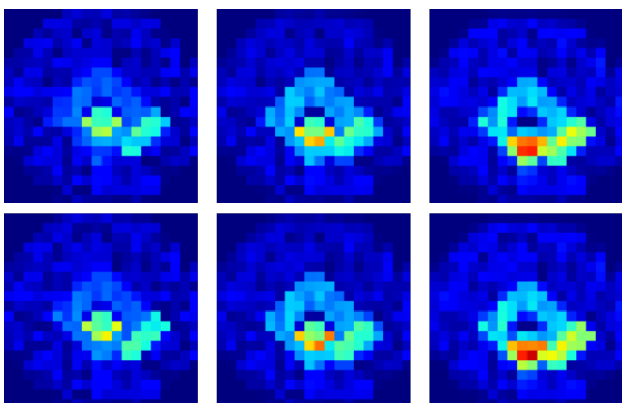


Figure 8. Generated images via trained projective network (top row) and the corresponding simulated radar images (bottom row): (left) $\theta = 15^\circ$, $\phi = 45^\circ$; (middle) $\theta = 30^\circ$, $\phi = 45^\circ$; (right) $\theta = 45^\circ$, $\phi = 45^\circ$.

4 Conclusion

This paper modeled the projection mechanism of radar system, and proposed a so-called projective network. Using only single example, it can learn a synthetic representation, which is then used for generating 2D RCS images under other observation angles. The comparison between the

reconstructed and ground truth images showed that the generated images have the similar profile as real ones, which verified the representation ability of proposed projective network. It reveals that physical-aware models have great potential for radar applications. Besides, the proposed network is differentiable. Thus it can be coupled with other neural network modules to boost the performance, which will be explored in the future.

However, the proposed model is a simplified one that can not be applied to practical radar data directly: 1) it assumes that the height of the target is known; 2) the shadow effect isn't considered in this paper; 3) the assumption of 3D RCS may not make sense in some cases. In the future, tools such as TensorFlow Graphics can be used and incorporated with computational electromagnetic methods to improve the model.

References

- [1] Q. Song and F. Xu, "Zero-Shot Learning of SAR Target Feature Space with Deep Generative Neural Networks," *IEEE Geoscience and Remote Sensing Letters*, **14**, 12, 2017.
- [2] J. Guo, B. Lei, C. Ding et al., "Synthetic Aperture Radar Image Synthesis by Using Generative Adversarial Nets," *IEEE Geoscience and Remote Sensing Letters*, **14**, 7, 2017.
- [3] Q. Song, F. Xu, and Y.-Q. Jin, "SAR Image Representation Learning with Adversarial Autoencoder Networks," *IEEE International Geoscience and Remote Sensing Symposium*, 2019.
- [4] P. Sibling, Y. Wang, S. Auer et al., "Generative Adversarial Networks for Synthesizing InSAR Patches," *arXiv preprint*, arXiv:2008.01184, 2020.
- [5] Z. Wei, and X. Chen, "Physics-inspired convolutional neural network for solving full-wave inverse scattering problems," *IEEE Transactions on Antennas and Propagation*, **67**, 9, pp. 6138–6148, 2019.
- [6] B. M. Lake, R. Salakhutdinov, J. B. Tenenbaum, "Human-level concept learning through probabilistic program induction," *Science*, **350**, 6266, pp. 1332–1338, 2015.
- [7] Z. Zhang, H. Wang, F. Xu et al., "Complex-valued convolutional neural network and its application in polarimetric SAR image classification," *IEEE Transactions on Geoscience and Remote Sensing*, **55**, 12, pp. 7177–7188, 2017.
- [8] B. Ding, G. Wen, and X. Huang et al., "Data Augmentation by Multilevel Reconstruction Using Attributed Scattering Center for SAR Target Recognition," *IEEE Geoscience and Remote Sensing Letters*, **14**, 6, pp. 979–983, 2017.